Frataxin Traps Low Abundance Quaternary Structure to Stimulate Human Fe-S Cluster Biosynthesis

Seth A. Cory[†,a], Cheng-Wei Lin[†,a], Steven M. Havens[a], Shachin Patra[a], Christopher D. Putnam[b], Mehdi Shirzadeh[a], David H. Russell[a] and David P. Barondeau*[,a]

[a]Department of Chemistry, Texas A&M University, College Station, TX 77842, USA.

[b]Department of Medicine, University of California School of Medicine, La Jolla, CA, 92093-0660, USA.

[†]Contributed equally to the manuscript

*To whom correspondence should be addressed: Department of Chemistry, Texas A&M University, College Station, TX 77842, USA. Telephone: 979-458-0735. E-mail: barondeau@tamu.edu

Keywords: Friedreich's ataxia, frataxin, iron-sulfur, ion mobility mass spectrometry, morpheein

Abstract

Iron-sulfur clusters are essential protein cofactors synthesized in human mitochondria by an NFS1-ISD11-ACP-ISCU2-FXN assembly complex. Surprisingly, researchers have discovered three distinct quaternary structures for cysteine desulfurase subcomplexes, which display similar interactions between NFS1-ISD11-ACP protomeric units but distinct dimeric interfaces between the protomers. Although the role of these different architectures is unclear, possible functions include regulating activity and promoting the biosynthesis of distinct sulfur-containing biomolecules. Here, crystallography, native ion-mobility mass spectrometry, and chromatography methods reveal the Fe-S assembly subcomplex exists as an equilibrium mixture of these different quaternary structures. Our results suggest Friedreich's ataxia (FRDA) protein frataxin (FXN) functions as a "molecular lock" and shifts the equilibrium towards one of the architectures to stimulate the cysteine desulfurase activity and promote iron-sulfur cluster biosynthesis. An NFS1-designed variant similarly shifts the equilibrium and partially replaces FXN in activating the complex. These results suggest that eukaryotic cysteine desulfurases are unusual members of the morpheein class of enzymes that control their activity through their oligomeric state. Overall, the findings support architectural switching as a regulatory mechanism linked to FXN activation of the human Fe-S cluster biosynthetic complex and provide new opportunities for therapeutic interventions of the fatal neurodegenerative disease FRDA.

Introduction

Iron-sulfur (Fe-S) clusters are essential inorganic cofactors found in proteins across all domains of life. These clusters play important roles in various biological processes, including oxidative respiration, DNA replication and repair, and catalytic transformations of substrates. The ISC biosynthetic pathway synthesizes Fe-S clusters in the mitochondria of eukaryotic cells and the cytosol for many prokaryotes.[1-3] However, the substrates required for their synthesis, S^{2-} and Fe^{2+}, contribute to oxidative stress by inhibiting respiratory complex IV and undergoing Fenton chemistry, respectively.[4,5] As a result, multiple levels of post-translational regulation control eukaryotic Fe-S cluster biosynthesis, and defects in this biosynthetic pathway can lead to disease.[6] These poorly understood regulatory mechanisms include the allosteric activator protein frataxin (FXN),[7-12] the metabolite sensing acyl-carrier protein (ACP),[13-16] and amino acid post-translational modifications.[17-19] Understanding the details of these mechanisms is crucial for a comprehensive understanding of Fe-S cluster biosynthesis and may provide valuable insights into therapeutic interventions for human diseases.

A multi-protein assembly complex located in the mitochondrial matrix is responsible for synthesizing Fe-S clusters. The sulfur-hub of the assembly system exists as a stable subcomplex consisting of the pyridoxal 5'-phosphate (PLP) dependent cysteine desulfurase (NFS1),[20,21] a member of the eukaryotic-specific LYRM superfamily (ISD11),[22-24] and ACP.[13,15,16] This subcomplex generates persulfide intermediates with subsequent transfer of the sulfane sulfur atoms to the scaffold protein ISCU2, where they are combined with ferrous iron and 2 electrons, likely provided by a ferredoxin protein,[25,26] to synthesize $[2Fe\text{-}2S]^{2+}$ clusters.[27] The cysteine desulfurase complex is also involved in other critical cellular processes, such as sulfur trafficking for molybdenum cofactor biosynthesis and tRNA modifications.[28-30] FXN binds to the assembly complex and stimulates Fe-S cluster biosynthesis.[7-12,25,27,31-33] Notably, the loss of FXN is linked to developing the neurodegenerative disease Friedreich's ataxia.[34] Despite the considerable progress made in understanding the individual chemical steps accelerated by FXN, it is imperative that we conduct further research to fully comprehend the structural basis and physiological purpose of this regulation.

Structural studies have identified three different quaternary structures for the eukaryotic cysteine desulfurase complex, which is composed of NFS1-ISD11 associated with *E. coli* ACP. This complex will be referred to as SDA_{ec} in this report. The first X-ray crystal structure exhibited an "open" architecture (Fig. 1A),[15] which differed dramatically from the prokaryotic homolog IscS. This open form exhibited an $\alpha_2\beta_2\gamma_2$ quaternary structure, where ISD11 molecules played a crucial role in mediating interactions between two NFS1-ISD11-ACP ($\alpha\beta\gamma$) protomers. The open architecture has few direct interactions between the NFS1 subunits, unlike the extensive subunit interactions observed in IscS.[35] A subsequent crystal structure revealed the SDA_{ec} complex can generate a second, distinct $\alpha_2\beta_2\gamma_2$ quaternary structure using an NFS1-NFS1 instead of an ISD11-ISD11 interface (Fig. 1B).[16] This "closed" SDA_{ec} architecture was also found to differ from the IscS-IscS dimer interface. When aligned, the two-fold axes show a 10° rotation of each NFS1 subunit in the closed SDA_{ec} dimer compared to its IscS counterpart. Further structural studies revealed that the SDA_{ec} complex can form a third "ready" architecture (Fig. 1C) upon binding of ISCU2 ($SDA_{ec}U$)[16] or

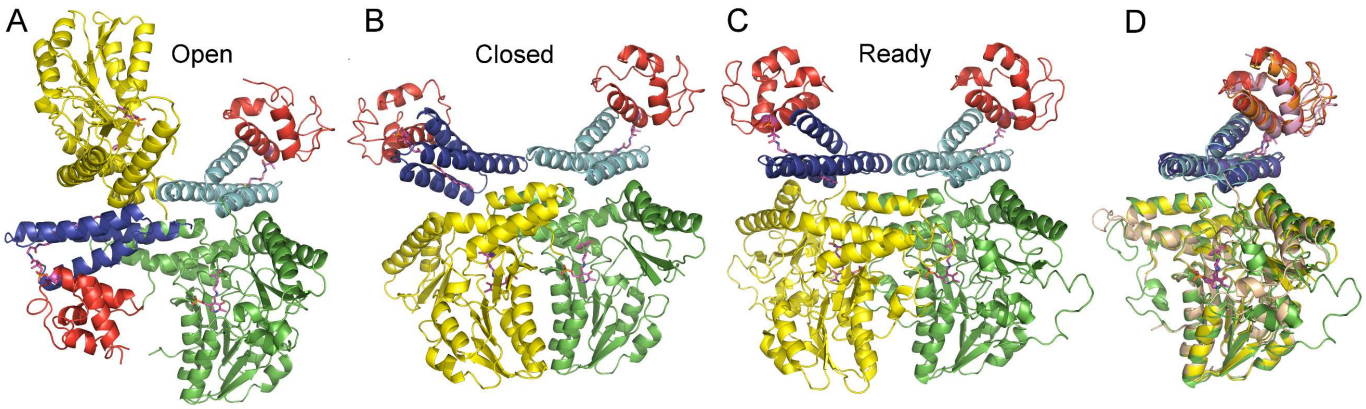

Figure 1. Comparison of different SDA_{ec} architectures. Structure of the SDA_{ec} complex in the (**A**) open (pdb: 5USR), (**B**) closed (pdb: 5WGB), and (**C**) ready (pdb: 6NZU; ISCU2 and FXN not shown) forms. NFS1 is shown in yellow and green, ISD11 in blue and cyan, and ACP_{ec} in red. The green/cyan/red protomer is shown in the same orientation for the different architectures. (**D**) Overlay of the subunits from one protomer for NFS1 (green, yellow, and wheat), ISD11 (cyan, blue, and purple), and ACP (red, orange, and pink) of the ready, closed, and open forms, respectively. Protein cofactors are shown in magenta.

both ISCU2 and FXN ($SDA_{ec}UF$).[36] The ready architecture uses the same interface between NFS1 subunits as is observed in the IscS dimer (Fig. S1). While the NFS1-ISD11-ACP_{ec} protomers are superimposable for the three forms (Fig. 1D), they use different protein-protein interactions to generate the open, closed, and ready SDA_{ec} architectures.

The formation of different quaternary structures using distinct protein-protein interfaces is not a common occurrence, and the physiological function of these different assemblies remains a topic of active research. The similarity of the dimer interface between the ready SDA_{ec} architecture and IscS suggests that the ready form is the functional architecture for Fe-S cluster biosynthesis.[16,36-38] However, the ready architecture doesn't provide a clear explanation for the essential functional requirement of ISD11, unlike the open architecture, which depends on ISD11 for protomer association (Fig. 1A). Additionally, the ready architecture, which has similar active site and protein-protein interactions with IscS, doesn't easily explain the low activity and need for an activator in the eukaryotic Fe-S cluster assembly system. Moreover, the ready form doesn't account for additional differences from the prokaryotic system, such as the distinct binding characteristics of accessory proteins with their respective cysteine desulfurases and opposing activation/inhibition effects of FXN homologs.[15,25,31,39-42] Interestingly, while small-angle X-ray scattering (SAXS) and crosslinking mass spectrometry studies provide evidence for the closed or ready form of the SDA_{ec} architecture in solution, other electron microscopy studies indicate that the open architecture is the predominant form for the SDA_{ec} complex.[15,16,43]

The eukaryotic Fe-S assembly complex has three architectures with distinct NFS1 active site conformations, reminiscent of the morpheein class of regulatory proteins. Morpheeins are known to control activity by shifting the equilibrium between different oligomeric forms that have distinct functionalities.[44] However, there is no evidence that multiple cysteine desulfurase architectures exist in equilibrium or that the different forms have different activity profiles. Here, we employed a range of functional and biophysical approaches to examine the solution states of the SDA_{ec} complex. Our findings support an architectural switching model as a regulatory mechanism associated with FXN

activation of the human Fe-S cluster biosynthetic complex. These results highlight the significance of understanding the conformational landscape of the SDA_{ec} complex, including the relationship between the open, closed, and ready forms and their roles in sulfur trafficking and the synthesis of sulfur-containing biomolecules.

Results

The SDA_{ec} Preparation Method Does Not Affect Activity. We first investigated if different preparation methods for the SDA_{ec} complex might favor different architectures and influence the activity profile of the enzyme. Previously, researchers used slightly different expression and purification conditions to produce the SDA_{ec} complex, which they then used to crystallize the complex in open and closed forms.[15,16] The open form was expressed in cells growing in an auto-induction media (herein named AI),[15] whereas the closed form was induced in cells growing in a rich Terrific Broth media (herein named TB).[16] The purification of the AI-prepared SDA_{ec} complex also includes additional steps. The SDA_{ec} samples prepared by these different methods did not significantly differ in catalytic properties when assayed under activated conditions (Fig. S2). SDA_{ec} prepared under the AI conditions had a k_{cat} of 9.3 ± 0.5 min^{-1} and a K_M for cysteine of 22 ± 5 μM. When prepared under the TB conditions, SDA_{ec} had a k_{cat} of 11 ± 0.4 min^{-1} and a K_M for cysteine of 20 ± 3 μM. These kinetic constants were consistent with each other and with previous reports,[7,15,31] suggesting that the preparation method does not substantially influence the activity profile of the SDA_{ec} sample.

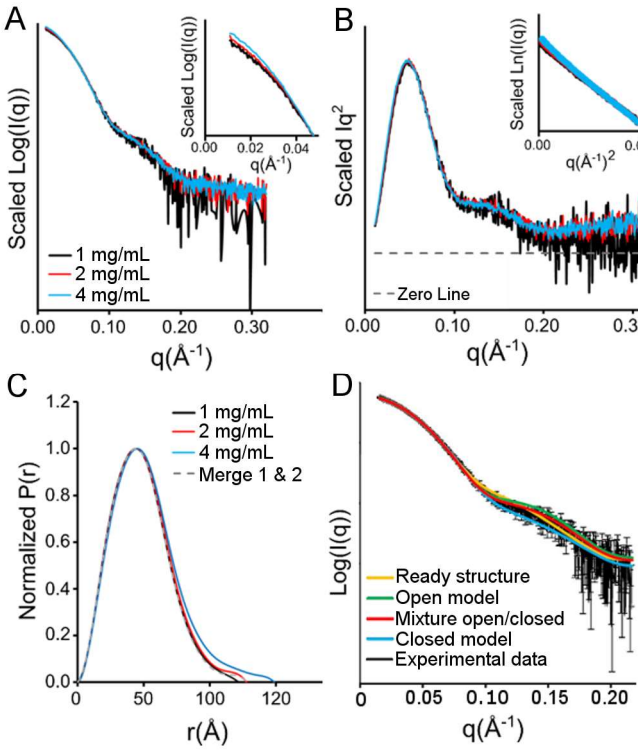

Figure 2. Small-angle X-ray scattering data for AI-prepared SDA_{ec}. The SDA_{ec} complex was prepared using the AI method and examined under high salt conditions. (**A**) Overlay of buffer-subtracted scattering curves. Inset: concentration dependent aggregation revealed by overlay of low q region. Negative intensities are not shown. (**B**) Kratky plots for SDA_{ec} at multiple concentrations. Inset: concentration dependent aggregation shown by Guinier plot analysis. (**C**) Pair distribution functions for SDA_{ec} samples. (**D**) Fits to the experimental data for the calculated scattering curves from the ready SDA_{ec} structure (yellow; χ^2 = 1.2), open model (green; χ^2 = 2.1) and closed model (blue; χ^2 = 2.1). The best two state model included the open (68%) and closed (32%) forms but did not improve the fit (red; χ^2 = 2.0).

Small-angle X-ray Scattering of SDA_{ec}. We then investigated if the different SDA_{ec} preparation methods affected the solution conformation. SAXS curves of the AI-prepared SDA_{ec} sample (Fig. 2) were collected, evaluated, and compared with previously analyzed SAXS samples generated with different preparation methods.[16,43] We found that a high ionic strength buffer containing glycerol and TCEP maximized the stability of the complex and reduced concentration-dependent aggregation (Fig. 2A).

Kratky plots of the scattering indicated that the samples were folded (Fig. 2B); however, we still observed minor concentration-dependent aggregation based on the behavior of the low q region of the scattering curve (Fig. 2A, inset) and the Guinier analysis (Fig. 2B, inset), as well as a concentration-dependent increase in D_{max} in the pair distribution function (Fig. 2C). Due to these observations, we analyzed the lowest concentration sample, which provided a smooth pair distribution function, a D_{max} approximately the diameter of all three SDA_{ec} architectures (100-110 Å), and a calculated[45] molecular weight that matched the expected molecular mass of 134 kDa (Table S1). Calculated scattering curves from the ready architecture, models of the open and closed forms, and mixtures of the different structures fit the experimental data similarly (Fig. 2D). Overall, fitting calculated scattering curves or SAXS *ab initio* reconstructions from these and additional models that included limited molecular dynamic simulations failed to be sufficiently deterministic to assign an architecture for the AI-prepared SDA_{ec}.

To compare our SAXS results with previous data from samples prepared by other groups, we reprocessed the scattering curves published by the Markley group,[43] obtained from SASBDB,[46] and the Cygler/Lill groups,[16] which they kindly provided. The data collected by the Markley group[43] closely resembled the data for our AI-prepared SDA_{ec} complex (Fig. S3A); the R_g from Guinier analysis was 36.3 Å and 36.9 Å (Table S1), respectively. The data collected by the Cygler/Lill groups[16] exhibited some concentration-dependent aggregation in the low q region (Fig. S3B). Our reanalysis of the Cygler/Lill data (Table S2) is consistent with their reported R_g of 54.7 Å and D_{max} of approximately 180 Å.[16] When we collected SAXS data with a lower ionic strength buffer comparable to that used by the Cygler/Lill groups, we obtained very similar scattering curves for our AI-prepared SDA_{ec} sample, an R_g of 51.5 Å and a D_{max} of approximately 189 Å (Fig. S3C and Table S2). Overall, the matching activity profiles and SAXS curves (Fig. S3, Table S1, and Table S2)[16,43] suggest that SDA_{ec} complexes prepared by the different groups have similar structure-function and solution properties.

Crystallization of Different SDA_{ec} Preparations in Both Open and Closed Forms. X-ray crystallography has provided the most substantial evidence of different SDA_{ec} architectures. We, therefore, investigated if the AI-prepared SDA_{ec} samples, used to generate crystals of the open architecture,[15] and TB-prepared SDA_{ec} samples, used to generate crystals of the closed architecture,[16] could generate both crystal forms. We buffer exchanged SDA_{ec} samples generated by the two methods and determined that each could be crystallized in the conditions for both the open and closed architectures (Fig. S4). We further verified the presence of both crystal forms by screening the

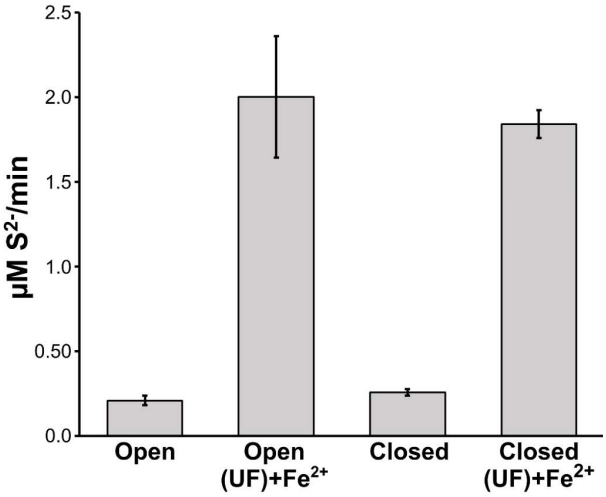

Figure 3. Isolated crystals in the open and closed forms exhibit similar cysteine desulfurase activities. Single crystals of the open and closed architectures were separately isolated, rinsed, and the resulting crystal slurries were dissolved by incubating with assay buffer at 37 °C for 15 min. The cysteine desulfurase activities of the open and closed samples were evaluated in the presence and absence of ISCU2, FXN, and Fe^{2+}. Error bars are replicate errors (n = 6).

crystals on an X-ray diffractometer. After indexing the screened images (Table S3), it was clear that regardless of the preparation method, the SDA_{ec} complex could be crystallized into forms corresponding to both the open and closed architectures, indicating that both architectures exist in solution or that the two architectures can interchange. Next, we tested the activity of samples generated from the crystals of the open and closed forms as a mechanism to "freeze out" the individual architectures. We selected single crystals of each architecture, washed them to remove residual protein, and dissolved them in an assay buffer to measure activity with and without the activator subunit FXN. Interestingly, samples generated from both open and closed crystals show the characteristic order of magnitude activation by FXN (Fig. 3). Together, these data indicate that the SDA_{ec} complex can exchange between open and closed forms or that both exist in solution. Moreover, these data suggest that adding FXN either activates both forms equally or, more likely, activates a single architecture generated by a quaternary structure rearrangement.

The SDA_{ec} Complex can Disassemble into Protomers and Undergo Exchange Reactions. The ability of SDA_{ec} samples to crystallize into both open and closed architectures led us to hypothesize that the distinct SDA_{ec} $\alpha_2\beta_2\gamma_2$ quaternary structures are in equilibrium. Based on the structures of the different architectures, interchange could occur via dissociation and reassociation of αβγ protomers or individual subunits. To test this hypothesis, we separately generated SDA_{ec} uniformly labeled with either ^{15}N or ^{14}N, mixed the two samples, and used native mass spectrometry to monitor if these complexes underwent subunit exchange reactions. Upon combining equimolar amounts of ^{15}N- and ^{14}N-labeled SDA_{ec}, an intermediate-mass species consistent with the exchange of entire αβγ protomers to generate a ^{15}N-SDA_{ec}-^{14}N-SDA_{ec} mixed complex was observed (Fig. S5). In contrast, we did not observe masses suggesting the exchange of individual subunits. The protomer exchange for SDA_{ec} reached an exchanged-to-unexchanged ratio of 0.83 at 120 min (Fig. 4; Table S4); the theoretical maximum for this ratio is 1.0, corresponding to a completely exchanged equimolar mixture. Next, we tested whether the His-tag influenced the SDA_{ec} protomer exchange reaction or the equilibrium between open, closed, and ready architectures. The protomer exchange reaction for SDA_{ec} lacking the His-tag on the NFS1 N-terminus was slower than the tagged material and required 24 hours to reach an exchanged-to-unexchanged ratio of 0.79 (Table S4). This result is consistent with the his-tag influencing either the dissociation of the SDA_{ec} complex to form αβγ

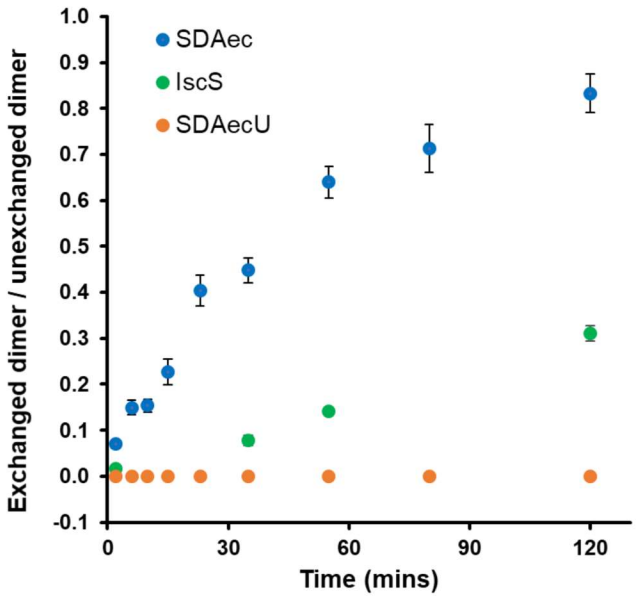

Figure 4. Protomer exchange for cysteine desulfurase complexes. Kinetics of an exchange reaction monitored by native mass spectrometry using a 1:1 ratio of His-tagged ^{14}N-SDA_{ec} ($^{14}N^{14}N$) and ^{15}N-SDA_{ec} ($^{15}N^{15}N$) complexes (blue). The Y axis is shown as the ratio of the amount of exchanged dimer ($^{15}N^{14}N$) divided by the sum of unexchanged dimer ($^{14}N^{14}N$ and $^{15}N^{15}N$). His-tagged and untagged versions of IscS undergo a similar exchange reaction monitored by native MS (green). Preincubation of ^{14}N-SDA_{ec} and ^{15}N-SDA_{ec} samples with ISCU2 completely inhibited the subsequent exchange reaction (orange). Error bars are replicate errors (n = 3).

protomers or the reassembly of $\alpha_2\beta_2\gamma_2$ complexes. To examine whether changes in the exchange reaction affected activity, we tested the ability of untagged SDA_{ec} to be activated by FXN in the presence of 1 mM L-cysteine and Fe^{2+} and found similar activation (unactivated = 1.30 ± 0.01 μM S^{2-}/min · μM NFS1; activated = 7.88 ± 0.34 μM S^{2-}/min · μM NFS1) to the tagged SDA_{ec}.[15] Similar native MS control experiments using the *E. coli* cysteine desulfurase IscS dimer with or without a His-tag revealed a slow exchange process (reaching an exchanged-to-unexchanged ratio of 0.31 at 120 min). Strikingly, pre-incubating saturating amounts of ISCU2 or ISCU2 plus FXN with the SDA_{ec} complex or IscU with IscS inhibited these exchange reactions (Fig. 4; Table S4). Together, these results reveal that the SDA_{ec} complex is dynamic and that the SDA_{ec} $\alpha_2\beta_2\gamma_2$ complexes can dissociate and reassemble $\alpha\beta\gamma$ protomers and suggests a model for switching between the open, closed, and ready architectures (see Discussion).

Interconvertible Forms of the SDA_{ec} Complex in Solution. We discovered that different forms of AI-prepared SDA_{ec} could be separated using a high-resolution cation exchange column. Native SDA_{ec} reproducibly separated into major (peak 3) and minor (peak 2) species (Fig. 5A). Next, we evaluated whether these species could interconvert. The major species (peak 3) was isolated, concentrated, diluted with the loading buffer, and then reinjected onto the column. This sample's elution profile included peaks 2 and 3 (Figs. S6A and S6B), suggesting conversion from the major to the minor species. These results indicate multiple SDA_{ec} forms are present in the solution, consistent with the ability to crystallize different architectures from the same sample (above), and interchange within minutes through a dynamic equilibrium process.

We hypothesize that the species separated by cation exchange chromatography correspond to different SDA_{ec} architectures. We tentatively assigned Peak 3 as the open architecture based on the predominance of the open form in SDA_{ec} solutions.[15] Peak 2 may be either or both closed and ready forms, as these architectures have similar surface charge properties. We designed the Q64S, P299H, and L300Q NFS1 variant (herein designated as SHQ) to shift the population from the open to the ready architecture and support these tentative assignments. These introduced SHQ residues are conserved in prokaryotic cysteine desulfurases and were expected to reduce steric clashes near the N-terminus and form new hydrogen bonds across the protein-protein interface of the ready form of the SDA_{ec} complex (Figs. S7 and S8). The SHQ variant exhibited an enhanced amount of peak 2 in cation exchange chromatography (Fig. 5B), consistent with the tentative assignment of the ready form. The SHQ variant also had a similar FXN-based stimulation in cysteine desulfurase activity (8 μM S^{2-}/min · μM

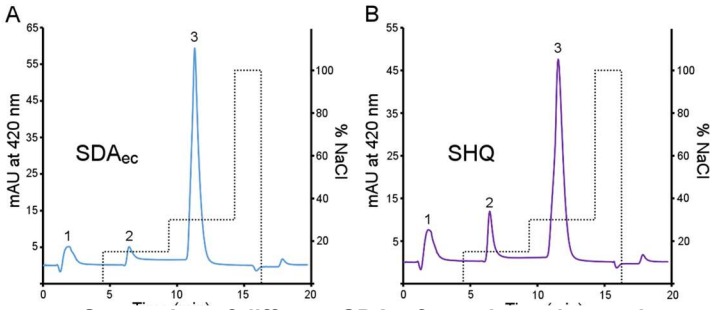

Figure 5. Separation of different SDA_{ec} forms by cation exchange chromatography. Different species were eluted for cysteine desulfurase samples from a cation exchange column using a step salt gradient. The PLP cofactor for SDA_{ec} samples was monitored at 420 nm. (**A**) The native SDA_{ec} sample (30 μM) had a major species that eluted at ~12 min (peak 3) and a minor species that eluted at ~7 min (peak 2). (**B**) The SHQ (30 μM) variant showed a larger initial population of peak 2 than SDA_{ec}. Note that peak 1 likely results from the premature elution of the species in peak 2 due to the inability to remove all the salt from the injected sample for stability purposes.

NFS1) to the native SDA_{ec} complex (Fig. S9). Notably, the SHQ variant had a 3-fold greater cysteine desulfurase activity than the native SDA_{ec} complex without FXN (Fig. S9). The increase in activity for the SHQ variant suggests the peak 2 species is the functional form of the complex. Overall, cation exchange chromatography revealed at least two SDA_{ec} species in solution that are interconvertible and appear to correlate with cysteine desulfurase activity.

FXN Converts the SDA_{ec} and $SDA_{ec}U$ Complexes from an Extended to a Compact Conformation. Next, we used native ion-mobility mass spectrometry (IM-MS) to investigate the conformational landscape and different architectures of the SDA_{ec} complex. IM-MS measures the arrival time of ions traveling through a drift tube filled with buffer gas molecules. Ions experience acceleration by an electric field and are slowed by collisions with gas molecules. Ions with a higher charge, a lower mass, or a compact shape travel faster through the drift cell. IM-MS charge state data for the SDA_{ec} complex revealed a large amount of a slower migrating (extended) form and a minor faster migrating (compact) species (Fig. 6). There was minor variability in the amount of slower and faster migrating forms of SDA_{ec} depending on the batch and the presence of the his-tag (Fig. S10A). Incubation of tagged and untagged SDA_{ec} samples at different temperatures before IM-MS analysis also slightly influenced the amount of extended and compact species (Fig. S10B). Charge reduction analyses are consistent with the slower migrating complex being a more extended native-like conformation rather than a collisionally activated species (Fig. S10C).

IM-MS analysis of the SHQ variant showed an enrichment of the faster migrating (compact) form compared to the SDA_{ec} complex (Fig. 6). Theoretical calculations (Table S5) indicate that the ready and closed forms of the SDA_{ec}

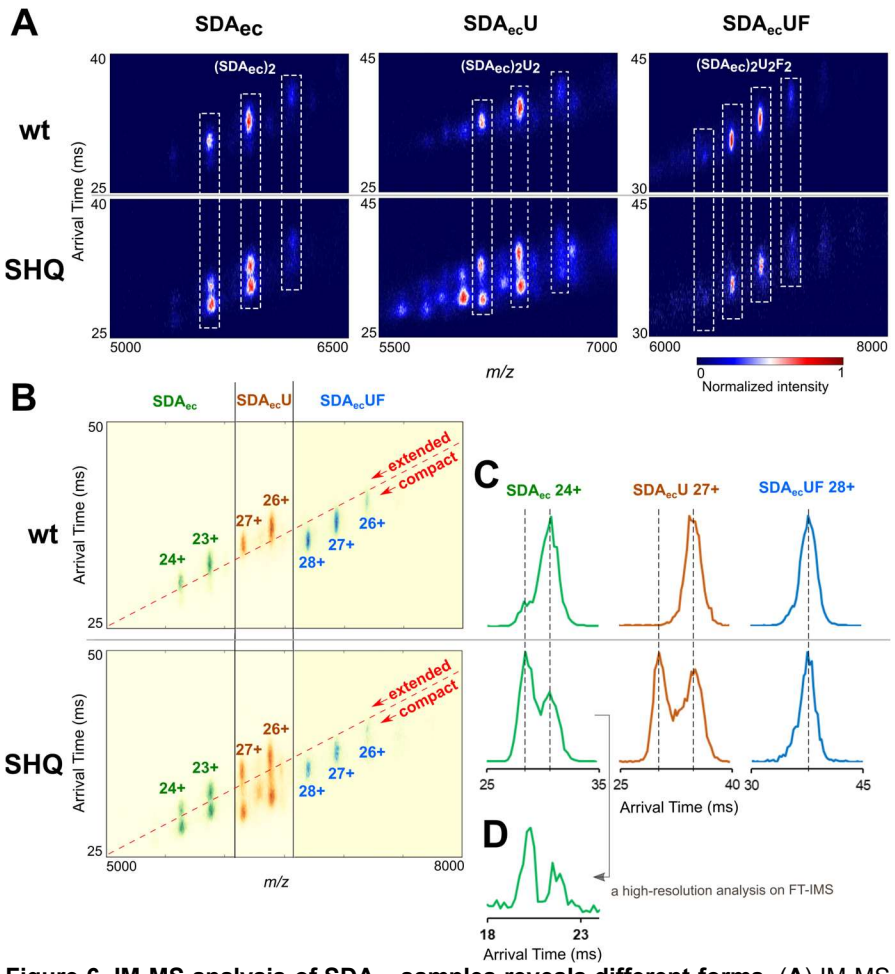

Figure 6. IM-MS analysis of SDA_{ec} samples reveals different forms. (**A**) IM-MS of native and variant SDA_{ec} as isolated complexes, in the presence of ISCU2, and with both ISCU2 plus FXN. (**B**) Overlaid IM-MS spectra from panel A. The SDA_{ec} and $SDA_{ec}U$ are predominantly in the slower migrating form (extended conformer trend line), whereas the $S^{SHQ}DA_{ec}$ and $S^{SHQ}DA_{ec}U$ are enriched in the faster migrating species (compact conformer trend line). $SDA_{ec}UF$ and $S^{SHQ}DA_{ec}UF$ exist as a single dominant species (compact conformer trend line). (**C**) Arrival time distribution of native and variant SDA_{ec} 24+, $SDA_{ec}U$ 27+, and $SDA_{ec}UF$ 28+. (**D**) Arrival time distribution of $S^{SHQ}DA_{ec}$ 24+ measured by the high-resolution FT-IMS instrument.

complex have similar collisional cross-sectional areas and are more compact than the open form.[47-52] These calculations are consistent with the assignment of the slower migrating (extended) species as the open architecture and the faster migrating (compact) species as the closed and ready forms. Overall, the results are consistent with the major peak in cation exchange and IM-MS experiments being a low-activity open architecture and the minor peak being a higher activity ready form.

Next, we assessed whether the addition of ISCU2 and FXN affected the relative amounts of the extended and compact species in IM-MS. The SDA_{ec} and SHQ variant complexes exhibit approximately the same amount of extended and compact forms with or without ISCU2 (Fig. 6), suggesting ISCU2 binds with similar affinity to the different forms. Strikingly, adding ISCU2 and FXN converts the SDA_{ec} and SHQ complexes to a single species following the faster-migrating trendline (Fig. 6), consistent with FXN preferentially binding to the compact form. These results, in combination with the activity of samples generated from crystals from the different architectures, protomer exchange, and cation separation assays, suggest a dynamic interconversion between eukaryotic cysteine desulfurase architectures that appear to be a critical part of the FXN activation phenomenon.

Discussion

Defining the physiological role and mechanistic details of FXN in the eukaryotic Fe-S assembly pathway has received significant attention due to its connection to Friedreich's ataxia (FRDA).[34] In 2010, *in vitro* assays revealed a role for FXN in stimulating the activity of the eukaryotic cysteine desulfurase complex.[7] More recent studies show that FXN accelerates chemical steps associated with the mobile S-transfer loop, including the decay of the Cys-quinonoid PLP intermediate, the accumulation of a persulfide species on NFS1, and the sulfur transfer reaction to ISCU2.[11,12] The analogous prokaryotic cysteine desulfurases, including the *E. coli* IscS that is 60% identical to NFS1, does not require the FXN-based activation and is functional without the additional subunits ISD11 and ACP, suggesting fundamental differences between the eukaryotic and prokaryotic cysteine desulfurases.

The SDA_{ec} crystal structure in the open architecture provided the first evidence that these differences manifested as dramatic structural changes in the eukaryotic cysteine desulfurases.[15] The open form features a solvent-exposed PLP, an incomplete substrate binding channel, and a quaternary structure that lacks significant NFS1-NFS1 interactions (Fig. 1A), which are a hallmark of prokaryotic IscS cysteine desulfurases (Fig. S1). A closed architecture crystal structure soon followed, revealing a significant NFS1-NFS1 interface[16] but with different protein-protein interactions than IscS.[35,37,38] Compared to IscS, the closed structure places the PLP cofactors 5 Å closer to one another and positions structural elements to potentially inhibit the function of the mobile loop cysteine in the sulfur transfer reaction (Fig. S11). Remarkably, structures that included ISCU2 or ISCU2 and FXN revealed a third ready form of the SDA_{ec} complex[16,36] with the same protein interface as IscS (Fig. S1). The relationship between these different architectures, their connection to FXN activation, and their functional roles in sulfur transfer reactions remain incompletely understood.

Here, we establish that the structure-function properties of SDA_{ec} samples are independent of the preparation method, that these samples consist of interconvertible equilibrium mixtures of

different species, and that variant complexes or the binding of additional subunits can shift this equilibrium between states. Crystallographic studies reveal SDA_{ec} samples exist as a mixture or can convert between the open and closed forms (Fig. S4 and Table S3). IM-MS and cation exchange chromatography results also indicate multiple components in SDA_{ec} samples with a qualitative correlation between faster (compact) and slower (extended) migrating species in IM-MS with eluting peaks 2 and 3 from the cation exchange column (Figs. 5 and 6). We assigned the slower migrating species in IM-MS as the open form and the faster migrating species as the closed and/or ready form based on a comparison of experimental and calculated collisional cross-sectional areas (Table S5). This assignment is consistent with the enriched open-form population for SDA_{ec} samples in negative stain electron microscopy studies.[15] IM-MS data also indicates that ISCU2 can bind to both extended and compact species of the SDA_{ec} complex and does not significantly shift the population between forms (Fig. 6). Although there are no structural snapshots of the open or closed SDA_{ec} forms bound to ISCU2, the ISCU2 binding sites in the ready architecture[16,36] are distant from the αβγ protomer interaction sites, suggesting that each architecture can bind ISCU2 (Fig. 7).

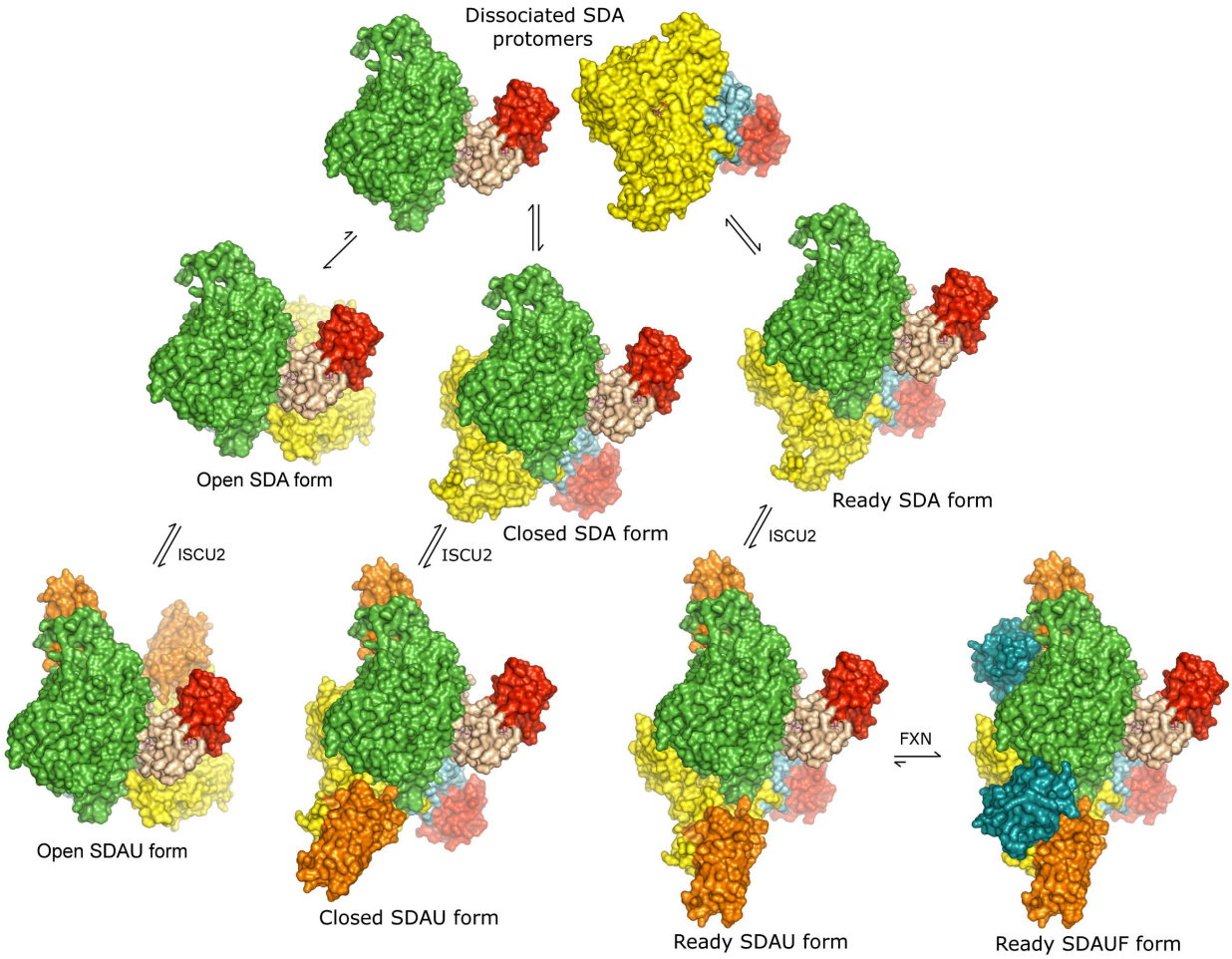

Figure 7. Morpheein model for the Fe-S cluster biosynthetic subcomplex. The NFS1-ISD11-ACP (SDA) complex exists as an equilibrium mixture of open (most abundant), closed, and ready architectures that are in equilibrium. ISCU2 binds to all three forms and does not significantly alter the equilibrium between forms. FXN binds to the SDAU ready form and locks the complex in the active conformation. NFS1 (green and yellow), ISD11 (wheat and cyan), ACP (red), ISCU2 (orange), and FXN (dark teal) subunits are shown as surfaces. The green NFS1 protomer is shown in the same orientation throughout the figure.

Our results support and extend an architectural switch model in which FXN drives a change in the quaternary structure to activate the cysteine desulfurase and Fe-S cluster assembly activities (Fig 7).[11] We provide evidence that SDA_{ec} samples exist as an equilibrium mixture of open, closed, and ready forms. Native mass spectrometry ^{15}N-^{14}N exchange assays show that SDA_{ec} samples can dissociate into $\alpha\beta\gamma$ protomers and reassemble into $\alpha_2\beta_2\gamma_2$ complexes (Fig. 4). Such a complex-protomer-complex conversion process provides a possible route to interconverting between open, closed, and ready architectures. The $\alpha\beta\gamma$ protomers are not observed with direct biophysical techniques, indicating the protomer-complex equilibrium favors $\alpha_2\beta_2\gamma_2$ complex formation, and suggests the SDA_{ec} complex's slow ^{15}N-^{14}N exchange kinetics may be due to low populations of ^{15}N-$\alpha\beta\gamma$ and ^{14}N-$\alpha\beta\gamma$ protomers, which need to coexist to produce a mixed isotope complex. It is unclear if ISCU2 must dissociate to form exchangeable SDA_{ec} species for the interconversion of $SDA_{ec}U$ architectures or if a similar complex-protomer-complex conversion occurs with $\alpha\beta\gamma\delta$ protomers. It is also unclear if the closed and ready forms can directly interconvert or if they must dissemble into protomers and reassemble. Our IM-MS data reveals that adding FXN converts the sample from existing as multiple species to one form, almost certainly the $SDA_{ec}UF$ observed in the cryo-EM structure.[36] We view FXN as a "molecular lock" that preferentially binds to the ready form and stitches the two protomers together by simultaneously binding with both NFS1 subunits. In contrast, similar FXN interactions with both NFS1 subunits in the other architectures are impossible due to a steric overlap with the rotated protomers in the closed form and the new ISD11-ISD11 protomer interface in the open form (Fig. S12). Driving the complex to the ready form would change the mobile S-transfer loop from a primarily disordered (open form) and potentially inhibited (closed form) to a functional trajectory (ready form) that promotes the PLP and sulfur transfer chemistry (Fig. S11). The inability of the sulfur acceptor protein ISCU2, unlike FXN, to shift the population of these different architectures is consistent with its failure to activate the SDA_{ec} complex.[7]

This type of global structural rearrangement is uncommon. The closest system that describes this process is the morpheein model. Morpheeins are enzymatic systems that are in a dynamic equilibrium with a variety of different oligomeric or architectural states. The equilibrium between states is allosterically regulated, and for one oligomer or architecture to convert to the other, the system must dissociate, undergo a conformational change, and then re-associate.[53] Similarly, we propose conformational differences in protomers dictate the equilibrium population of the open, closed, and ready architectures. Stabilizing one of the quaternary structures over the others shifts the equilibrium and function of the complex (Fig. 7). We tested this hypothesis by designing the SHQ variant, which showed enhanced activity and changes in IM-MS and cation exchange results consistent with a shifted population away from the open form and towards a closed or ready form. The equilibrium position also appears to be influenced by the sample incubation temperature (Fig. S10). Small molecule effectors typically regulate human morpheein systems, and clinical mutations affect oligomeric distributions and activities for morpheein systems.[54-57] In the human cysteine desulfurase system, a small molecule effector has not been identified, but FXN functions to alter the oligomeric distribution by locking the complex in the active form for Fe-S cluster biosynthesis. It will be interesting to evaluate whether clinical variants of NFS1, ISD11, ISCU2, and FXN[58-63] alter the equilibrium between different architectures or potentially fail to lock the complex in the active form.

In summary, these and previous studies provide substantial evidence that the eukaryotic cysteine desulfurase is a morpheein-like system that controls activity by its oligomeric form (Table S6). Assigning structure-function properties for the different architectures will require thoughtfully designed biochemical probes and high-resolution structural analysis. One possibility is that these architectures are part of a protein assembly-based regulatory mechanism that controls sulfur transfer from the SDA_{ec} complex to acceptor proteins for Fe-S cluster assembly, molybdenum cofactor biosynthesis, and tRNA modifications. Overall, we have provided new insights into the relationship between the eukaryotic cysteine desulfurase architectures and the mechanism of FXN activation that have implications for regulating Fe-S cluster assembly. Finally, the ability of the SHQ variant to partially replace FXN function by shifting the population of quaternary structures suggests that molecules that drive a similar architectural switch may have potential applications as FRDA therapeutics.

Materials and Methods

Protein Preparation and Purification

Preparation of SDA_{ec}. The NFS1(Δ1-55)-ISD11(S11A)-ACP_{ec} (SDA_{ec}) was prepared following the published procedures describing the open[15] and closed[16] architectures. The two procedures used identical expression constructs that encode an N-terminal His_6 tag on NFS1, which was not cleaved unless indicated. The two preparation methods differed in expression conditions, using auto-induction (AI conditions)[15] or Terrific Broth (TB conditions)[16] media, and slightly different purification procedures. A tobacco etch virus (TEV) protease cleavage site was introduced by mutagenesis into the original NFS1 plasmid to generate material with a cleavable His_6 tag. The purification was conducted as previously described[15] with a 4 °C overnight TEV cleavage step introduced after the cation exchange column to generate cleaved SDA_{ec}. The digested product, which contained a single glycine residue before residue 56, was loaded onto a Ni-NTA column (5 mL; GE Healthcare) to remove the TEV protease. To generate ^{15}N-labeled SDA_{ec}, 2 – 6 liters of N-5052 auto-induction media[64] were inoculated with 8 mL of an overnight LB starter culture. The ^{15}N-SDA_{ec} complex was purified as previously described[15], except that supplemental pyridoxal 5'-phosphate was not added during the preparation. The QuikChange protocol (Agilent) was used to introduce the Q64S L299H P300Q substitutions into the NFS1 plasmid (pet-15b).[15] SDA_{ec} variants were purified using the same protocol as the native enzyme complex. The concentrations for the SDA_{ec} complexes were determined using an extinction coefficient of 10.9 mM^{-1} cm^{-1} at 420 nm.

Preparation of ISCU2 and FXN. A MEGAWHOP protocol[65] was used to incorporate a TEV protease site and glutathione S-transferase (GST) into a pET-30a(+) vector containing ISCU2 (Δ1-35) and generate the C-terminally tagged construct *ISCU2-TEV-GST*. Further mutagenesis was used to incorporate a C-terminal His_6 tag to produce the *ISCU2-TEV-GST-His_6* construct. The *ISCU2-TEV-GST* plasmid was transformed into the E. coli strain BL21(DE3) for expression. Cells were grown at 37 °C to an OD_{600} of 0.5. Protein expression was induced with 0.1 mM isopropyl β-D-1-thiogalactopyranoside (IPTG) at 18 °C. Cells were grown overnight, harvested by centrifugation the following morning, and stored in a -80 °C freezer until use. The cell pellet from a 9 L culture was thawed and resuspended in GST buffer A (50 mM Hepes, 150 mM NaCl, pH = 7.8). Lysozyme (20

mg, Sigma-Aldrich) and protease inhibitor cocktail (20 mg, Sigma-Aldrich) were added to the suspension. The cells were lysed by two cycles of French press at 18,500 psi. Cell debris was cleared by centrifugation at 16,420 RCF for 30 min. The clarified lysate was loaded onto a manually packed GST-column (Prometheus) at 4 °C. Bound protein was eluted with GST buffer B (50 mM Hepes, 150 mM NaCl, 10 mM glutathione (GSH), pH = 7.8). The TEV digestion was conducted overnight at 4 °C, and the products were loaded onto a Ni-NTA column (5 mL; GE Healthcare) to remove the TEV protease. The flow-through from the Ni-NTA column was concentrated to 20 mL, diluted to 150 mL with cation A buffer (50 mM Hepes, pH = 7.8), and loaded onto a cation exchange column (27 mL; POROS 50HS, Applied Biosystems) and eluted with a linear gradient of NaCl (0 – 1 M). The fractions containing ISCU2 were concentrated, brought into an anaerobic Mbraun glovebox (~12 °C, <1 ppm O_2 as monitored by a Teledyne model 310 analyzer), and supplemented with 5 mM D,L-dithiothreitol (DTT) before loading onto a HiPrep 26/60 Sephacryl S100 HR column (GE Healthcare Life Sciences) equilibrated in size exclusion buffer (50 mM Hepes, 150 mM NaCl, pH = 7.5). The fractions corresponding to monomeric ISCU2 were collected, concentrated, and flash-frozen in liquid nitrogen for storage at -80 °C until use. For the *ISCU2-TEV-GST-His$_6$* construct, the same procedure was used except that the cation exchange step was skipped. The preparation of FXN (Δ1-81) gene was previously described.[66] Concentrations for ISCU2 and FXN were determined using extinction coefficients of 9970 and 26,930 $M^{-1}cm^{-1}$ at 280 nm, respectively, as estimated by ExPASy ProtParam.[67]

Preparation of IscU and IscS. The *E. coli* proteins IscU and IscS were expressed and purified as previously described.[31] The extinction coefficient of 6.6 mM^{-1} cm^{-1} at 388 nm was used to estimate the concentration of the PLP cofactor, which represented the concentration of active IscS, in 0.1 M NaOH. The extinction coefficient of 11,460 M^{-1} cm^{-1} at 280 nm was used to estimate the concentration of IscU.

Activity Measurements of Purified Complexes

The cysteine desulfurase activity was determined using the methylene blue assay as previously described[15] in assay buffer (50 mM Hepes, 250 mM NaCl, pH = 7.5). Reaction mixtures of 800 µL contained the following components: 0.5 µM SDA_{ec} (or the SHQ variant), 1.5 µM ISCU2, 1.5 µM FXN, 4 mM D,L-DTT, and 5 µM $(NH_4)_2Fe(SO_4)_2$ were incubated at 37 °C for 15 min before the addition of varying amounts of L-cysteine. Reactions were quenched after 6 mins and the sulfide was quantified as previously described. The sulfide formation rate for each L-cysteine concentration was measured at least in triplicate. Data were fit using KaleidaGraph (Synergy Software) to a traditional Michaelis-Menten equation. The errors in the Michaelis-Menten parameters represent errors in the fit to the experimental data. FXN binding was evaluated as previously described.[60]

Preparation of the SDA_{ec} Complex for Small-Angle X-ray Scattering

Purified AI-prepared SDA_{ec} was injected onto a Superdex 200 10/300 GL column (S200, GE Healthcare Life Sciences) equilibrated in 50 mM Hepes, 250 mM NaCl, pH = 7.2 to remove any aggregates from the freeze/thaw cycle of the sample. Yellow fractions were collected, pooled, and concentrated to approximately 10 mg/mL. Dialysis buttons (Hampton Research) were loaded with

50 µL of sample and sealed with a 3.5 kDa dialysis membrane disc (Hampton Research, Spectrum) that had been washed thoroughly with Milli-Q H_2O. Samples were then dialyzed into various buffers in 50 mL falcon tubes overnight at 4 °C before diluting within a 96-well plate. High salt conditions were defined as 100 mM sodium phosphate, 500 mM NaCl, 2% glycerol, 2 mM TCEP, pH = 8.0. Low salt conditions included 50 mM Hepes, 250 mM NaCl, 2 % glycerol, 2 mM TCEP, pH = 7.5. The 96-well plate containing samples was sealed and shipped wrapped in ice packs to the SIBYLS beamline (12.3.1) at the Advanced Light Source (ALS). The plate was stored at 4 °C and was centrifuged at 3700 rpm for 10 minutes before data collection. Data collection parameters can be found in Table S7.

Small-Angle X-ray Scattering Data Collection and Analysis

Individual buffers and frames were analyzed for consistency. Buffers with the same composition and scattering profile were averaged using the ATSAS 2.8.4[68] package to generate an average buffer scattering curve. Sample frames were then individually subtracted from the averaged buffer in the RAW 1.5.1 package.[69,70] Subtracted frames were then averaged in RAW at different time points to determine the onset of radiation damage. Exposure times, which included the least amount of radiation damage, were used for further analysis. The low q region was truncated based on Guinier analysis, and the high q region was truncated to $8/R_g$ prior to the pair distribution analysis. Additional information regarding Guinier analysis, pair-distribution function analysis, and curve fitting can be found in Tables S1 and S2. We used the same procedure to reanalyze the Markley and Cygler/Lill SAXS data, except that the scattering curve was truncated in the Guinier region due to significant aggregation[16] or interference from the beamstop[43]. Because the crystal structures of the open[15] and closed[16] SDA_{ec} architectures lacked a substantial number of non-hydrogen protein scatterers due to disordered regions in crystal structures (17.2% and 31.6%, respectively), we generated more complete models for calculating SAXS profiles by overlaying the NFS1-ISD11-ACP protomers (αβγ) of the cryo-EM ready form[36] onto the open and closed architectures. The model for the ready architecture was generated by removing the ISCU2 and FXN subunits from the cryo-EM SDA_{ec}UF structure.[36]

Crystallization of SDA_{ec} from Different Preparation Methods

The open and closed forms of SDA_{ec} were crystallized as previously described[15,16] using the AI-preparation and TB-preparation methods, respectively. A hanging-drop vapor diffusion method was used that included 500 µL of crystallization solutions in the well and a 4 µL drop (2 µL protein: 2 µL crystallization solution) on the coverslip. The AI-prepared SDA_{ec} in the closed form was prepared for crystallization by buffer exchanging the protein complex into 10 mM BIS-TRIS (pH 5.5), 200 mM NaCl, 20 mM KCl, 2 mM NaH_2PO_4, 2 mM Na_2HPO_4, 5 % (vol/vol) glycerol, 1 mM D,L-DTT, and 75 mM imidazole by multiple rounds of concentration and dilution using a Vivaspin 500 100 kDa spin concentrator (GE Healthcare). The TB-prepared SDA_{ec} in the open form was prepared for crystallization by buffer exchanging the protein complex into 50 mM Hepes, 250 mM NaCl, 10 % glycerol, pH = 7.5 or injected onto a Superdex 200 10/300 GL column (S200, GE Healthcare Life Sciences) equilibrated in 50 mM Hepes, 250 mM NaCl, 10 % glycerol, pH = 7.5. The AI-prepared

SDA_{ec} (177 μM) was crystallized in the open architecture at 22 °C with crystallization conditions generated by adding 5 mL of 40% acetone to 11.25 mL of 0.1 M CBTP (pH = 6.4), 0.3 M CsCl, 0.2 M D,L-allylglycine, 5 mM TCEP, and 8% PEG 3350. The AI-prepared SDA_{ec} (177 μM) without D,L-allylglycine was crystallized in the open architecture at 22 °C with crystallization conditions generated by adding 1.25 mL of 40 % acetone to 11.25 mL of 0.1 M CBTP (pH = 6.4), 0.3 M CsCl, 5 mM TCEP, and 8 % PEG 3350. The AI-prepared SDA_{ec} (220 μM) and the TB-prepared SDA_{ec} (226 μM) were crystallized in the closed architecture at 12 °C using a crystallization solution of 0.1 M MES (pH = 6.5), 0.3 M ammonium acetate, 0.02 M calcium acetate hydrate, 0.02 M calcium chloride dihydrate, and 15 % isopropanol. The TB-prepared SDA_{ec} (177 μM) was crystallized in the open architecture at 22 °C using a crystallization solution of 0.1 M CBTP (pH = 6.4), 0.2 M CsCl, 0.2 M D,L-allylglycine, 5 mM TCEP, 10 % PEG 3350, and 4 % acetone.

X-ray Data Collection, Indexing, and Unit Cell Determinations

Single crystals of SDA_{ec} in the open architecture were harvested and cryo-protected as previously described[15] using a final concentration of 20 % (vol/vol) PEG 400. Crystal trays of SDA_{ec} in the closed architecture were transferred to a 17 °C room where single crystals were harvested and cryo-protected as previously described.[16] Diffraction data were collected using a rotating anode Cu K-α source and a Rigaku R-AXIS IV detector. Specifically, two images for each crystal form were collected at 2Θ = 0° and 90° at a temperature of 120 K with an exposure time of 6 min, detector distance ranging from 200 to 250 mm, and an oscillation angle ranging from 0.5° to 0.2° depending on the diffraction quality. Indexing was performed with iMosflm[71] version 7.2.2 from the CCP4[72] package. The unit cell parameters were automatically chosen by iMosflm.

Activity Analysis of Single Crystals

Crystals of SDA_{ec}, in either form, were harvested from four separate drops. Wash solution (10 μL of assay buffer) was first added to each drop and then the crystals were transferred to a 200 μL solution of assay buffer. Single crystals from the 200 μL drop were transferred to a seeding tool where the crystals were crushed to generate a slurry. The slurry was brought into an anaerobic glovebox, where the activity measurements were conducted. A total of six alternating reactions (150 μL) with and without the additional subunits and Fe^{2+} were performed by mixing 20 μL of crystal slurry, additional subunits (3 μM), Fe^{2+} (10 μM), and D,L-DTT (4 mM) together and incubating at 37 °C for 15 minutes. The reactions were initiated by the addition of L-cysteine to a final concentration of 1 mM. A quench solution of 37.5 μL of a 1:1 mixture of 20 mM *N*,*N*-dimethyl-p-phenylenediamine in 7.2 N HCl and 30 mM $FeCl_3$ in 1.2 N HCl was added to the sample after 10 minutes. Sulfide concentration was determined as described above. Two independent triplicate runs were conducted, totaling six measurements for each sample.

Native Mass Spectrometry Experiments

Native mass spectrometry (Native MS) was performed on two instruments for different purposes: an Exactive Plus with extended mass range (EMR) Orbitrap MS (Thermo Fisher Scientific,

San Jose, CA) for high-resolution measurements or a Synapt G2 instrument (Waters Corporation, U.K.) equipped with an 8k RF generator for ion mobility measurements. Gold-coated tips prepared using a Sutter 1000 were used for nano-electrospray ionization experiments.[73] Fresh protein samples, including SDA_{ec}, ISCU2, FXN, IscS, and IscU, were buffer exchanged into 200 mM ammonium acetate (pH = 8.5) using Micro Bio-Spin 6 Columns (Bio-Rad). Experimental and expected masses can be found in Table S8. All calculated masses excluded the N-terminal methionine (if present in the sequence). The calculated masses of SDA_{ec} and SDA_{ec} complexes included the mass of the covalently attached PLP and the assumed mass of the acyl-4'PPT ACP_{ec} was 523 Da. Masses of SDA_{ec}/SDA_{ec}U/SDA_{ec}UF/ISCU2/FXN were measured under native conditions (200 mM ammonium acetate, pH = 8.5). Masses of SDA_{ec} subunits were also measured under denaturing conditions (1% formic acid). All masses were measured using the EMR.

Protomer Exchange Experiments Using Native Mass Spectrometry

Protomer exchange experiments were performed on an EMR Orbitrap MS. The high resolution of EMR gives resolved peaks between subunit mixtures for quantification purposes. Instrument parameters were tuned to minimize collisional activation while retaining reasonable signal-to-noise. The mass spectrometer parameters used were set as: m/z range 3000-10000, capillary temperature 200-300 °C, S-Lens RF level 200, source DC offset 25 V, injection flatapole DC 16 V, inter flatapole lens DC 12 V, bent flatapole DC 7-12 V, transfer multipole DC offset 7-10 V, C-trap entrance lens tune offset 0 V, trapping gas pressure setting 7, in-source dissociation voltage 0 eV, HCD collision energy 10 eV, FT resolution 8750–35000, positive ion mode, and ion maximum injection time 50–200 ms. For SDA_{ec} exchange experiments, a 1:1 ratio of ^{15}N-SDA_{ec} and ^{14}N-SDA_{ec} were mixed to initiate the exchange reaction. For subunit exchange of SDA_{ec}U, ^{15}N-SDA_{ec} and ^{14}N-SDA_{ec} were incubated with ISCU2 distinctly using a 1:3 ratio for 30 min to form ^{15}N-SDA_{ec}U and ^{14}N-SDA_{ec}U complexes ($\alpha_2\beta_2\gamma_2\delta_2$). These complexes were mixed in a 1:1 ratio to initiate the exchange reaction. For the exchange of SDA_{ec}UF, ^{15}N-SDA_{ec} and ^{14}N-SDA_{ec} were incubated with ISCU2 and FXN distinctly using a 1:3:3 ratio for 30 minutes to form ^{15}N-SDA_{ec}UF and ^{14}N-SDA_{ec}UF complexes ($\alpha_2\beta_2\gamma_2\delta_2\varepsilon_2$). ^{14}N-$SDA_{ec}$UF and ^{15}N-$SDA_{ec}$UF were mixed in a 1:1 ratio to initiate the exchange reactions. The exchange of tagged IscS and untagged IscS was also investigated using a 1:1 ratio. For subunit exchange of IscS-IscU, tagged IscS and untagged IscS were incubated with IscU distinctly using a 1:3 ratio for 30 minutes to form untagged IscS-IscU and tagged IscS-IscU complexes ($\alpha_2\beta_2$). The exchange reaction was initiated by mixing untagged IscS-IscU and tagged IscS-IscU complexes at a 1:1 ratio. At various time points, aliquots (4 uL) were taken for native MS analysis. Each spectrum was taken for 20 seconds. The initial MS data were collected using the Thermo Exactive software under the RAW format. The protein species were deconvoluted using the software program UniDec.[74] All the exchange experiments were performed at room temperature.

Cation Exchange Column Separation of SDA_{ec} Species.

The native and variant SDA_{ec} samples were thawed rapidly and diluted to 60 μM with 50 mM HEPES, 250 mM NaCl, 10 % glycerol, pH 7.5. The samples were diluted in half with cation buffer A (50 mM HEPES, 20 mM NaCl, 2 % glycerol, pH 8.0) to a final concentration of 30 μM. Samples (1

mL) were injected onto a Mono S 5/50 GL (GE Healthcare) column using either a BioRad Quest or an AKTA FPLC and eluted using a step gradient of cation buffer B (50 mM Hepes, 1 M NaCl, 2 % glycerol, pH 8) with steps at 15 %, 30 %, and 100 %. For equilibrium experiments, the peak selected for isolation was concentrated to ~400 – 500 µL using a 100 kDa cutoff Vivaspin 500 (GE Healthcare) by centrifugation at 10,000 RCF. The remaining sample was diluted to 1 mL with cation buffer A and reinjected and eluted using the same procedure. All experiments were performed at room temperature.

Ion-mobility Mass Spectrometry of SDA_{ec}/$SDA_{ec}U$/$SDA_{ec}UF$

Native ion-mobility mass spectrometry (Native IM-MS) was performed on a Synapt G2 instrument. Instrument parameters were tuned to maximize ion intensity but simultaneously preserve the native-like state of proteins as determined by IM. The instrument was set to a capillary voltage of 1-1.5 kV, source temperature of 30 °C, sampling cone voltage of 10 V, extraction cone voltage of 1 V, trap and transfer collision energy off, and backing pressure (5 mbar), trap flow rate at 8 ml/min, He cell flow rate at 200 ml/min, IMS flow rate at 50 ml/min. The T-wave settings for trap (310 ms^{-1}/6.0 V), IMS (250 ms^{-1}/9-12 V) and transfer (65 ms^{-1}/2 V), and trap bias (25.0 V). MassLynx 4.1 (Waters) and Pulsar were used to deconvolute all recorded mass spectra.[75] A sodium iodide solution was used to externally calibrate mass spectra. Experimental collisional cross-section (CCS) of ^{14}N tagged SDA_{ec} (134.2 kDa), ^{14}N untagged SDA_{ec} (129.3 kDa), $SDA_{ec}U$ (using ^{14}N tagged SDA_{ec}, 164.9 kDa), $SDA_{ec}UF$ (using ^{14}N tagged SDA_{ec}, 193.3 kDa) were determined following a well-documented protocol and a CCS database.[76,77] Calibration curves (R^2 >0.978) were generated by using solutions of transthyretin (55.6 kDa), concanavalin A (103.0 kDa), and pyruvate kinase (237 kDa). Parameters for calculating the CCS using the online projected superposition approximation (PSA) webserver (psa.chem.fsu.edu) were set as follows: buffer gas of nitrogen, a temperature of 298 K, projection accuracy of 0.01, projection integration accuracy as 0.009, shape accuracy as 0.01, shape maxiter as 25, and shape meshfactor as 1.[48,50,51] The models used for calculating the CCS were generated as described above.

Additional Software and Figure Generation

Plots were generated in either Excel (Microsoft) or KaliedaGraph (Synergy Software). Structural figures were generated using Chimera 1.11.2[78] or PyMOL 2.4[79]. High-resolution artboards and figures were developed using Inkscape (https://inkscape.org/) and GIMP (https://www.gimp.org/).

ACKNOWLEDGMENTS

We would like to thank Seth Van Andel and Adam Hillaire for comments on the manuscript and Kathryn Burnett for collecting the high throughput SAXS measurements at SIBYLS beamline 12.3.1 of the Advanced Light Source (ALS). We would also like to thank Dr. James Sacchettini for use of the X-ray diffraction equipment. Support for this work was funded by the NIH grants R01GM096100 (D.P.B.), R01GM121751 (D.H.R.), and P41GM128577 (D.H.R.) plus the Robert A. Welch grant A-1647 (D.P.B). This work was conducted ALS, a national user facility operated by

Lawrence Berkeley National Laboratory on behalf of the Department of Energy, Office of Basic Energy Sciences, through the Integrated Diffraction Analysis Technologies (IDAT) program, supported by DOE Office of Biological and Environmental Research. Additional support comes from the National Institute of Health project ALS-ENABLE (P30 GM124169) and a High-End Instrumentation Grant S10OD018483.

References

1 Roche, B. *et al.* Iron/sulfur proteins biogenesis in prokaryotes: formation, regulation and diversity. *Biochim Biophys Acta* **1827**, 455-469 (2013). https://doi.org/10.1016/j.bbabio.2012.12.010

2 Braymer, J. J. & Lill, R. Iron-sulfur cluster biogenesis and trafficking in mitochondria. *J Biol Chem* **292**, 12754-12763 (2017). https://doi.org/10.1074/jbc.R117.787101

3 Zheng, L., Cash, V. L., Flint, D. H. & Dean, D. R. Assembly of iron-sulfur clusters. Identification of an iscSUA-hscBA-fdx gene cluster from Azotobacter vinelandii. *J Biol Chem* **273**, 13264-13272 (1998). https://doi.org/10.1074/jbc.273.21.13264

4 Jiang, J. *et al.* Hydrogen Sulfide--Mechanisms of Toxicity and Development of an Antidote. *Sci Rep* **6**, 20831 (2016). https://doi.org/10.1038/srep20831

5 Fenton, H. J. H. LXXIII.—Oxidation of tartaric acid in presence of iron. *J. Chem. Soc., Trans.* **65**, 899-910 (1894). https://doi.org/10.1039/ct8946500899

6 Rouault, T. A. & Tong, W. H. Iron-sulfur cluster biogenesis and human disease. *Trends Genet* **24**, 398-407 (2008). https://doi.org/10.1016/j.tig.2008.05.008

7 Tsai, C. L. & Barondeau, D. P. Human frataxin is an allosteric switch that activates the Fe-S cluster biosynthetic complex. *Biochemistry* **49**, 9132-9139 (2010). https://doi.org/10.1021/bi1013062

8 Das, D., Patra, S., Bridwell-Rabb, J. & Barondeau, D. P. Mechanism of frataxin "bypass" in human iron-sulfur cluster biosynthesis with implications for Friedreich's ataxia. *J Biol Chem* **294**, 9276-9284 (2019). https://doi.org/10.1074/jbc.RA119.007716

9 Bridwell-Rabb, J., Fox, N. G., Tsai, C. L., Winn, A. M. & Barondeau, D. P. Human frataxin activates Fe-S cluster biosynthesis by facilitating sulfur transfer chemistry. *Biochemistry* **53**, 4904-4913 (2014). https://doi.org/10.1021/bi500532e

10 Parent, A. *et al.* Mammalian frataxin directly enhances sulfur transfer of NFS1 persulfide to both ISCU and free thiols. *Nat Commun* **6**, 5686 (2015). https://doi.org/10.1038/ncomms6686

11 Patra, S. & Barondeau, D. P. Mechanism of activation of the human cysteine desulfurase complex by frataxin. *Proc Natl Acad Sci U S A* **116**, 19421-19430 (2019). https://doi.org/10.1073/pnas.1909535116

12 Gervason, S. *et al.* Physiologically relevant reconstitution of iron-sulfur cluster biosynthesis uncovers persulfide-processing functions of ferredoxin-2 and frataxin. *Nat Commun* **10**, 3566 (2019). https://doi.org/10.1038/s41467-019-11470-9

13 Van Vranken, J. G. *et al.* The mitochondrial acyl carrier protein (ACP) coordinates mitochondrial fatty acid synthesis with iron sulfur cluster biogenesis. *Elife* **5**, e17828 (2016). https://doi.org/10.7554/eLife.17828

14 Van Vranken, J. G. *et al.* ACP Acylation Is an Acetyl-CoA-Dependent Modification Required for Electron Transport Chain Assembly. *Mol Cell* **71**, 567-580 e564 (2018). https://doi.org/10.1016/j.molcel.2018.06.039

15 Cory, S. A. *et al.* Structure of human Fe-S assembly subcomplex reveals unexpected cysteine desulfurase architecture and acyl-ACP-ISD11 interactions. *Proc Natl Acad Sci U S A* **114**, E5325-E5334 (2017). https://doi.org/10.1073/pnas.1702849114

16 Boniecki, M. T., Freibert, S. A., Muhlenhoff, U., Lill, R. & Cygler, M. Structure and functional dynamics of the mitochondrial Fe/S cluster synthesis complex. *Nat Commun* **8**, 1287 (2017). https://doi.org/10.1038/s41467-017-01497-1
17 Rocha, A. G. *et al.* Cysteine desulfurase is regulated by phosphorylation of Nfs1 in yeast mitochondria. *Mitochondrion* **40**, 29-41 (2018). https://doi.org/10.1016/j.mito.2017.09.003
18 Song, J. Y., Marszalek, J. & Craig, E. A. Cysteine desulfurase Nfs1 and Pim1 protease control levels of Isu, the Fe-S cluster biogenesis scaffold. *Proc Natl Acad Sci U S A* **109**, 10370-10375 (2012). https://doi.org/10.1073/pnas.1206945109
19 Ciesielski, S. J., Schilke, B., Marszalek, J. & Craig, E. A. Protection of scaffold protein Isu from degradation by the Lon protease Pim1 as a component of Fe-S cluster biogenesis regulation. *Mol Biol Cell* **27**, 1060-1068 (2016). https://doi.org/10.1091/mbc.E15-12-0815
20 Li, J., Kogan, M., Knight, S. A., Pain, D. & Dancis, A. Yeast mitochondrial protein, Nfs1p, coordinately regulates iron-sulfur cluster proteins, cellular iron uptake, and iron distribution. *J Biol Chem* **274**, 33025-33034 (1999). https://doi.org/10.1074/jbc.274.46.33025
21 Kispal, G., Csere, P., Prohl, C. & Lill, R. The mitochondrial proteins Atm1p and Nfs1p are essential for biogenesis of cytosolic Fe/S proteins. *EMBO J* **18**, 3981-3989 (1999). https://doi.org/10.1093/emboj/18.14.3981
22 Adam, A. C., Bornhovd, C., Prokisch, H., Neupert, W. & Hell, K. The Nfs1 interacting protein Isd11 has an essential role in Fe/S cluster biogenesis in mitochondria. *EMBO J* **25**, 174-183 (2006). https://doi.org/10.1038/sj.emboj.7600905
23 Wiedemann, N. *et al.* Essential role of Isd11 in mitochondrial iron-sulfur cluster synthesis on Isu scaffold proteins. *EMBO J* **25**, 184-195 (2006). https://doi.org/10.1038/sj.emboj.7600906
24 Shi, Y., Ghosh, M. C., Tong, W. H. & Rouault, T. A. Human ISD11 is essential for both iron-sulfur cluster assembly and maintenance of normal cellular iron homeostasis. *Hum Mol Genet* **18**, 3014-3025 (2009). https://doi.org/10.1093/hmg/ddp239
25 Webert, H. *et al.* Functional reconstitution of mitochondrial Fe/S cluster synthesis on Isu1 reveals the involvement of ferredoxin. *Nat Commun* **5**, 5013 (2014). https://doi.org/10.1038/ncomms6013
26 Cai, K., Tonelli, M., Frederick, R. O. & Markley, J. L. Human Mitochondrial Ferredoxin 1 (FDX1) and Ferredoxin 2 (FDX2) Both Bind Cysteine Desulfurase and Donate Electrons for Iron-Sulfur Cluster Biosynthesis. *Biochemistry* **56**, 487-499 (2017). https://doi.org/10.1021/acs.biochem.6b00447
27 Fox, N. G., Chakrabarti, M., McCormick, S. P., Lindahl, P. A. & Barondeau, D. P. The Human Iron-Sulfur Assembly Complex Catalyzes the Synthesis of [2Fe-2S] Clusters on ISCU2 That Can Be Transferred to Acceptor Molecules. *Biochemistry* **54**, 3871-3879 (2015). https://doi.org/10.1021/bi5014485
28 Leimkuhler, S., Buhning, M. & Beilschmidt, L. Shared Sulfur Mobilization Routes for tRNA Thiolation and Molybdenum Cofactor Biosynthesis in Prokaryotes and Eukaryotes. *Biomolecules* **7** (2017). https://doi.org/10.3390/biom7010005
29 Marelja, Z., Stocklein, W., Nimtz, M. & Leimkuhler, S. A novel role for human Nfs1 in the cytoplasm: Nfs1 acts as a sulfur donor for MOCS3, a protein involved in molybdenum cofactor biosynthesis. *J Biol Chem* **283**, 25178-25185 (2008). https://doi.org/10.1074/jbc.M804064200
30 Noma, A., Sakaguchi, Y. & Suzuki, T. Mechanistic characterization of the sulfur-relay system for eukaryotic 2-thiouridine biogenesis at tRNA wobble positions. *Nucleic Acids Res* **37**, 1335-1352 (2009). https://doi.org/10.1093/nar/gkn1023
31 Bridwell-Rabb, J., Iannuzzi, C., Pastore, A. & Barondeau, D. P. Effector role reversal during evolution: the case of frataxin in Fe-S cluster biosynthesis. *Biochemistry* **51**, 2506-2514 (2012). https://doi.org/10.1021/bi201628j

32 Pandey, A. *et al.* Frataxin directly stimulates mitochondrial cysteine desulfurase by exposing substrate-binding sites, and a mutant Fe-S cluster scaffold protein with frataxin-bypassing ability acts similarly. *J Biol Chem* **288**, 36773-36786 (2013). https://doi.org/10.1074/jbc.M113.525857
33 Colin, F. *et al.* Mammalian frataxin controls sulfur production and iron entry during de novo Fe4S4 cluster assembly. *J Am Chem Soc* **135**, 733-740 (2013). https://doi.org/10.1021/ja308736e
34 Campuzano, V. *et al.* Friedreich's ataxia: autosomal recessive disease caused by an intronic GAA triplet repeat expansion. *Science* **271**, 1423-1427 (1996). https://doi.org/10.1126/science.271.5254.1423
35 Cupp-Vickery, J. R., Urbina, H. & Vickery, L. E. Crystal structure of IscS, a cysteine desulfurase from Escherichia coli. *J Mol Biol* **330**, 1049-1059 (2003). https://doi.org/10.1016/s0022-2836(03)00690-9
36 Fox, N. G. *et al.* Structure of the human frataxin-bound iron-sulfur cluster assembly complex provides insight into its activation mechanism. *Nat Commun* **10**, 2210 (2019). https://doi.org/10.1038/s41467-019-09989-y
37 Shi, R. *et al.* Structural basis for Fe-S cluster assembly and tRNA thiolation mediated by IscS protein-protein interactions. *PLoS Biol* **8**, e1000354 (2010). https://doi.org/10.1371/journal.pbio.1000354
38 Marinoni, E. N. *et al.* (IscS-IscU)2 complex structures provide insights into Fe2S2 biogenesis and transfer. *Angew Chem Int Ed Engl* **51**, 5439-5442 (2012). https://doi.org/10.1002/anie.201201708
39 Adinolfi, S. *et al.* Bacterial frataxin CyaY is the gatekeeper of iron-sulfur cluster formation catalyzed by IscS. *Nat Struct Mol Biol* **16**, 390-396 (2009). https://doi.org/10.1038/nsmb.1579
40 Fox, N. G., Das, D., Chakrabarti, M., Lindahl, P. A. & Barondeau, D. P. Frataxin Accelerates [2Fe-2S] Cluster Formation on the Human Fe-S Assembly Complex. *Biochemistry* **54**, 3880-3889 (2015). https://doi.org/10.1021/bi5014497
41 Yan, R. *et al.* Ferredoxin competes with bacterial frataxin in binding to the desulfurase IscS. *J Biol Chem* **288**, 24777-24787 (2013). https://doi.org/10.1074/jbc.M113.480327
42 Kim, J. H., Frederick, R. O., Reinen, N. M., Troupis, A. T. & Markley, J. L. [2Fe-2S]-ferredoxin binds directly to cysteine desulfurase and supplies an electron for iron-sulfur cluster assembly but is displaced by the scaffold protein or bacterial frataxin. *J Am Chem Soc* **135**, 8117-8120 (2013). https://doi.org/10.1021/ja401950a
43 Cai, K., Frederick, R. O., Dashti, H. & Markley, J. L. Architectural Features of Human Mitochondrial Cysteine Desulfurase Complexes from Crosslinking Mass Spectrometry and Small-Angle X-Ray Scattering. *Structure* **26**, 1127-1136 e1124 (2018). https://doi.org/10.1016/j.str.2018.05.017
44 Jaffe, E. K. Morpheeins--a new structural paradigm for allosteric regulation. *Trends Biochem Sci* **30**, 490-497 (2005). https://doi.org/10.1016/j.tibs.2005.07.003
45 Rambo, R. P. & Tainer, J. A. Accurate assessment of mass, models and resolution by small-angle scattering. *Nature* **496**, 477-481 (2013). https://doi.org/10.1038/nature12070
46 Valentini, E., Kikhney, A. G., Previtali, G., Jeffries, C. M. & Svergun, D. I. SASBDB, a repository for biological small-angle scattering data. *Nucleic Acids Res* **43**, D357-363 (2015). https://doi.org/10.1093/nar/gku1047
47 Wyttenbach, T., Bleiholder, C., Anderson, S. E. & Bowers, M. T. A new algorithm to characterise the degree of concaveness of a molecular surface relevant in ion mobility spectrometry. *Molecular Physics* **113**, 2344-2349 (2015). https://doi.org/10.1080/00268976.2015.1042935
48 Bleiholder, C., Contreras, S., Do, T. D. & Bowers, M. T. A novel projection approximation algorithm for the fast and accurate computation of molecular collision cross sections (II). Model parameterization and definition of empirical shape factors for proteins. *Int J Mass Spectrom* **345-347**, 89-96 (2013). https://doi.org/10.1016/j.ijms.2012.08.027

49 Wyttenbach, T., Bleiholder, C. & Bowers, M. T. Factors contributing to the collision cross section of polyatomic ions in the kilodalton to gigadalton range: application to ion mobility measurements. *Analytical chemistry* **85**, 2191-2199 (2013). https://doi.org/10.1021/ac3029008

50 Anderson, S. E., Bleiholder, C., Brocker, E. R., Stang, P. J. & Bowers, M. T. A novel projection approximation algorithm for the fast and accurate computation of molecular collision cross sections (III): Application to supramolecular coordination-driven assemblies with complex shapes. *Int J Mass Spectrom* **330-332**, 78-84 (2012). https://doi.org/10.1016/j.ijms.2012.08.024

51 Bleiholder, C., Wyttenbach, T. & Bowers, M. T. A novel projection approximation algorithm for the fast and accurate computation of molecular collision cross sections (I). Method. *Int J Mass Spectrom* **308**, 1-10 (2011). https://doi.org/10.1016/j.ijms.2011.06.014

52 McCabe, J. W. *et al.* First-Principles Collision Cross Section Measurements of Large Proteins and Protein Complexes. *Analytical chemistry* **92**, 11155-11163 (2020). https://doi.org/10.1021/acs.analchem.0c01285

53 Jaffe, E. K. & Lawrence, S. H. The morpheein model of allostery: evaluating proteins as potential morpheeins. *Methods Mol Biol* **796**, 217-231 (2012). https://doi.org/10.1007/978-1-61779-334-9_12

54 Sen, S. & Banerjee, R. A pathogenic linked mutation in the catalytic core of human cystathionine beta-synthase disrupts allosteric regulation and allows kinetic characterization of a full-length dimer. *Biochemistry* **46**, 4110-4116 (2007). https://doi.org/10.1021/bi602617f

55 Jaffe, E. K. & Lawrence, S. H. Allostery and the dynamic oligomerization of porphobilinogen synthase. *Arch Biochem Biophys* **519**, 144-153 (2012). https://doi.org/10.1016/j.abb.2011.10.010

56 Tang, L. *et al.* Single amino acid mutations alter the distribution of human porphobilinogen synthase quaternary structure isoforms (morpheeins). *J Biol Chem* **281**, 6682-6690 (2006). https://doi.org/10.1074/jbc.M511134200

57 Jaffe, E. K., Stith, L., Lawrence, S. H., Andrake, M. & Dunbrack, R. L., Jr. A new model for allosteric regulation of phenylalanine hydroxylase: implications for disease and therapeutics. *Arch Biochem Biophys* **530**, 73-82 (2013). https://doi.org/10.1016/j.abb.2012.12.017

58 Lim, S. C. *et al.* Mutations in LYRM4, encoding iron-sulfur cluster biogenesis factor ISD11, cause deficiency of multiple respiratory chain complexes. *Hum Mol Genet* **22**, 4460-4473 (2013). https://doi.org/10.1093/hmg/ddt295

59 Farhan, S. M. *et al.* Exome sequencing identifies NFS1 deficiency in a novel Fe-S cluster disease, infantile mitochondrial complex II/III deficiency. *Mol Genet Genomic Med* **2**, 73-80 (2014). https://doi.org/10.1002/mgg3.46

60 Bridwell-Rabb, J., Winn, A. M. & Barondeau, D. P. Structure-function analysis of Friedreich's ataxia mutants reveals determinants of frataxin binding and activation of the Fe-S assembly complex. *Biochemistry* **50**, 7265-7274 (2011). https://doi.org/10.1021/bi200895k

61 Tsai, C. L., Bridwell-Rabb, J. & Barondeau, D. P. Friedreich's ataxia variants I154F and W155R diminish frataxin-based activation of the iron-sulfur cluster assembly complex. *Biochemistry* **50**, 6478-6487 (2011). https://doi.org/10.1021/bi200666h

62 Coelho, M. P. *et al.* Iron-sulfur cluster ISD11 deficiency (LYRM4 gene) presenting as cardiorespiratory arrest and 3-methylglutaconic aciduria. *JIMD Rep* **49**, 11-16 (2019). https://doi.org/10.1002/jmd2.12058

63 Kollberg, G. *et al.* Clinical manifestation and a new ISCU mutation in iron-sulphur cluster deficiency myopathy. *Brain* **132**, 2170-2179 (2009). https://doi.org/10.1093/brain/awp152

64 Studier, F. W. Protein production by auto-induction in high density shaking cultures. *Protein Expr Purif* **41**, 207-234 (2005). https://doi.org/10.1016/j.pep.2005.01.016

65 Miyazaki, K. MEGAWHOP cloning: a method of creating random mutagenesis libraries via megaprimer PCR of whole plasmids. *Methods Enzymol* **498**, 399-406 (2011). https://doi.org/10.1016/B978-0-12-385120-8.00017-6
66 McCabe, J. W. *et al.* Variable-Temperature Electrospray Ionization for Temperature-Dependent Folding/Refolding Reactions of Proteins and Ligand Binding. *Analytical chemistry* **93**, 6924-6931 (2021). https://doi.org/10.1021/acs.analchem.1c00870
67 Wilkins, M. R. *et al.* Protein identification and analysis tools in the ExPASy server. *Methods Mol Biol* **112**, 531-552 (1999). https://doi.org/10.1385/1-59259-584-7:531
68 Franke, D. *et al.* ATSAS 2.8: a comprehensive data analysis suite for small-angle scattering from macromolecular solutions. *J Appl Crystallogr* **50**, 1212-1225 (2017). https://doi.org/10.1107/S1600576717007786
69 Nielsen, S. S. *et al.* BioXTAS RAW, a software program for high-throughput automated small-angle X-ray scattering data reduction and preliminary analysis. *J Appl Crystallogr* **42**, 959-964 (2009). https://doi.org/10.1107/s0021889809023863
70 Hopkins, J. B., Gillilan, R. E. & Skou, S. BioXTAS RAW: improvements to a free open-source program for small-angle X-ray scattering data reduction and analysis. *J Appl Crystallogr* **50**, 1545-1553 (2017). https://doi.org/10.1107/S1600576717011438
71 Battye, T. G., Kontogiannis, L., Johnson, O., Powell, H. R. & Leslie, A. G. iMOSFLM: a new graphical interface for diffraction-image processing with MOSFLM. *Acta Crystallogr D Biol Crystallogr* **67**, 271-281 (2011). https://doi.org/10.1107/S0907444910048675
72 Winn, M. D. *et al.* Overview of the CCP4 suite and current developments. *Acta Crystallogr D Biol Crystallogr* **67**, 235-242 (2011). https://doi.org/10.1107/S0907444910045749
73 Laganowsky, A. *et al.* Membrane proteins bind lipids selectively to modulate their structure and function. *Nature* **510**, 172-175 (2014). https://doi.org/10.1038/nature13419
74 Marty, M. T. *et al.* Bayesian deconvolution of mass and ion mobility spectra: from binary interactions to polydisperse ensembles. *Analytical chemistry* **87**, 4370-4376 (2015). https://doi.org/10.1021/acs.analchem.5b00140
75 Allison, T. M. *et al.* Quantifying the stabilizing effects of protein-ligand interactions in the gas phase. *Nat Commun* **6**, 8551 (2015). https://doi.org/10.1038/ncomms9551
76 Ruotolo, B. T., Benesch, J. L., Sandercock, A. M., Hyung, S. J. & Robinson, C. V. Ion mobility-mass spectrometry analysis of large protein complexes. *Nat Protoc* **3**, 1139-1152 (2008). https://doi.org/10.1038/nprot.2008.78
77 Bush, M. F. *et al.* Collision cross sections of proteins and their complexes: a calibration framework and database for gas-phase structural biology. *Analytical chemistry* **82**, 9557-9565 (2010). https://doi.org/10.1021/ac1022953
78 Pettersen, E. F. *et al.* UCSF Chimera--a visualization system for exploratory research and analysis. *J Comput Chem* **25**, 1605-1612 (2004). https://doi.org/10.1002/jcc.20084
79 Schrodinger, LLC. *The PyMOL Molecular Graphics System, Version 1.8* (2015).